Biogeosciences Discuss., 11, 18189–18227, 2014
www.biogeosciences-discuss.net/11/18189/2014/
doi:10.5194/bgd-11-18189-2014

Biogeosciences Discussions
Open Access

Emergence of multiple ocean ecosystem drivers in a large ensemble suite with an earth system model

K. B. Rodgers[1], **J. Lin**[2], **and T. L. Frölicher**[3]

[1]Program in Atmospheric and Oceanic Sciences, Princeton University, Princeton, USA
[2]Princeton University, Princeton, USA
[3]Environmental Physics, Institute of Biogeochemistry and for Pollutant Dynamics, ETH Zürich, Switzerland

Received: 6 December 2014 – Accepted: 8 December 2014 – Published: 21 December 2014

Correspondence to: K. B. Rodgers (krodgers@princeton.edu)

Published by Copernicus Publications on behalf of the European Geosciences Union.

Abstract

Marine ecosystems are increasingly impacted by human-induced changes. Ocean ecosystem drivers – including warming, acidification, deoxygenation and perturbations to biological productivity – can co-occur in space and time, but detecting their trends is complicated by the presence of noise associated with natural variability in the climate system. Here we use Large Initial-Condition Ensemble Simulations with a comprehensive Earth System Model under a historical/RCP8.5 pathway over 1950–2100 to consider emergence characteristics for the four individual and combined drivers. Using a one-standard deviation (67 % confidence) threshold of signal-to-noise to define emergence with a 30 yr trend window, we show that ocean acidification emerges much earlier than other drivers, namely during the 20th century over most of the global ocean. For biological productivity, the anthropogenic signal does not emerge from the noise over most of the global ocean before the end of the 21st century. The early emergence pattern for sea surface temperature in low latitudes is reversed from that of subsurface oxygen inventories, where emergence occurs earlier in the Southern Ocean. For the combined multiple-driver field, 41 % of the global ocean exhibits emergence for the 2005–2014 period, and 63 % for the 2075–2084 period. The combined multiple-driver field reveals emergence patterns by the end of this century that are relatively high over much of the Southern Ocean, North Pacific, and Atlantic, but relatively low over the tropics and the South Pacific. In regions with pronounced emergence characteristics, marine ecosystems can be expected to be pushed outside of their comfort zone determined by the degree of natural background variability to which they are adapted. The results here thus have implications not only for optimization of the ocean observing system, but also for risk assessment and mitigation strategies.

BGD
11, 18189–18227, 2014

1 Introduction

An important priority in climate research is to understand the potential vulnerabilities of marine ecosystems in the face of anthropogenic climate change (e.g. Doney et al., 2012). Over the last decade, multiple drivers of marine ecosystems such as ocean warming, ocean acidification, nutrient stress and low oxygen levels have been identified to be among those of greatest concern (e.g. Gruber, 2011; Hall et al., 2013). We have chosen to use "drivers" rather than the commonly used terminology "stressors" as some drivers (for example temperature) can be beneficial to some organisms or processes. On a global scale, the development of the drivers considered here is largely a consequence of the increase in atmospheric CO_2 and the associated climate change. The oceanic response to these changes, namely the oceanic uptake of excess heat and anthropogenic CO_2 causes ocean warming and ocean acidification, i.e. a decrease in both oceanic pH and in the saturation state of seawater with regard to mineral calcium carbonate (Doney et al., 2009). The warming of the ocean tends to stratify the upper ocean (Sarmiento et al., 1998), possibly leading to a reduced supply of nutrients to the euphotic zone (Bopp et al., 2001, Steinacher et al., 2010), but also to a reduced resupply of oxygen to the ocean's interior (Frölicher et al., 2009; Keeling et al., 2010), causing a loss of oxygen there. The magnitude of these global ecosystem drivers will likely continue to grow, given current trends in fossil fuel CO_2 emissions and the strong inertia within the global community with respect to efforts to decarbonize (Friedlingstein et al., 2014).

The detection of secular trends in ecosystem driver fields on regional- to global-scales is complicated by the presence of natural variability in the climate system, as has been shown for dissolved oxygen by Frölicher et al. (2009). The presence of background natural variability motivates the introduction of the concept of emergence to identify where the signal (the secular trend) becomes larger than the noise (the background natural variability). Identifying and understanding when and where the secular trends in ecosystem drivers emerge above the noise is important for two reasons. The

BGD
11, 18189–18227, 2014

first reason is that emergence characterizes when the secular trend becomes evident or perceptible for the local marine species relative to the background variability to which they have adapted. Here emergence becomes a measure of perceptible changes for the ecosystems. The second reason is that understanding of the emergence of multiple ecosystem drivers will be important for optimizing the design of the ocean observing system. Inferring trends in ecosystem drivers from Repeat Hydrography is complicated by natural variability in the ocean (Rodgers et al., 2009), and natural variability can also complicate trend detection using time series data (Henson et al., 2014).

Previous studies exploring the concept of emergence have largely focused on physical state variables of the atmosphere and ocean, such as temperature, precipitation and sea level (e.g. Diffenbaugh and Scherer, 2011; Hawkins and Sutton, 2012; Mahlstein et al., 2012; Mora et al., 2013; Lyu et al., 2014). Mora et al. (2013), for example emphasized that the tropics, which hold the worlds greatest diversity of marine species, will exhibit emergence in ocean warming ten years earlier than any of the other global ocean regions. Far less attention has been devoted to date to signal-to-noise ratios in ocean biogeochemistry, a notable exception being the study of Keller et al. (2014).

Here we introduce a new suite of Large Initial-Condition Ensemble Simulations using a comprehensive Earth System Model to understand the local emergence characteristics of the ocean ecosystem drivers sea surface temperature (SST), sea water saturation state with respect to aragonite (Ω_{arag}), the integrated oxygen content of the upper ocean (O_2 inventories), and net primary productivity (NPP) over an interdecadal (30 year) timescale. The ocean state as expressed in SST exhibits pronounced decadal-to-interdecadal variability (Zhang et al., 1997), and variations on this timescale are well documented for oxygen (Emerson et al., 2004; Mecking et al., 2008; Kouketsu et al., 2010; Takatani et al., 2012). This has also been considered for the case of phytoplankton in the study of Martinez et al. (2009). Given that analysis of emergence requires specifying a timescale over which trends are considered, we are motivated to

BGD
11, 18189–18227, 2014

focus on a 30 yr timescale here by the complications imposed by the observed power at decadal-to-interdecadal timescales.

In opting to use a suite of Large Initial-Condition Ensemble Simulations, we emphasize in particular the uncertainty in estimates of emergence due to natural variability inherent in the climate system. Deconvolving the signature of the forced response from the background natural variability with one coupled model requires Large Initial-Condition Ensemble Simulations. Only with a sufficiently large number of ensemble members can the effects of natural variability be removed by averaging over the ensemble members. With a single model run of a coupled climate model one is forced to estimate noise either from simulated pre-industrial variability or through high-pass filtering of a scenario run (e.g. Deser et al., 2014). The problem is that the forced response is in general imbedded in a stochastic dynamical system that exhibits variability on all timescales. Additionally, the amplitude of major modes of variability such as El Nino-Southern Oscillation (ENSO) is not stationary in their amplitude over climate change timescales (Timmermann et al., 1999). The ensemble approach to coupled modeling thereby offers an important opportunity when applied to the case of ecosystem drivers (Frölicher et al., 2009).

2 Methods

2.1 Model and simulations

We conducted 30 ensemble simulations over the 1950–2100 period following historical and RCP8.5 concentration pathways (van Vuuren et al., 2011). All 30 ensemble members are run with the same coupled Earth System Model developed at the Geophysical Fluid Dynamics Laboratory (Dunne et al., 2012, 2013): GFDL's ESM2M. The physical state model underlying ESM2M is the updated version of the coupled model CM2.1 (Delworth et al., 2006), consisting of the 1-degree version of the MOM4p1 ocean model (Griffies, 2009) coupled to an approximately 2-degree configuration of the AM2 atmo-

BGD
11, 18189–18227, 2014

spheric model (Anderson et al., 2004). The ocean biogeochemical model is Tracers of Ocean Phytoplankton and Allometric Zooplankton code version 2 including 30 tracers to represent cycles of carbon, oxygen, and the major macronutrients and iron (Dunne et al., 2010).

The initial conditions for the 30 ensemble members for 1 January 1950 differed in the initial state of the atmospheric component of the Earth System Model. This was accomplished by using model state snapshot for the ends of days 1–29 in January 1950 as the initial model states for 1 January 1950 for each of the ensemble members 2–30. As has been shown by Wittenberg et al. (2014) using significantly smaller initial perturbations with nearly the same underlying physical coupled model, our initial condition perturbation lead to a randomization of the ENSO state amongst the individual ensemble members within five years. Given that decadal modulations of ENSO are the most pronounced driver of decadal physical variability in this coupled model, decadal variability will be randomized amongst the individual ensemble members.

The four ecosystem drivers considered in this study are (i) surface sea water saturation state with respect to aragonite (Ω_{arag}), a mineral phase of calcium carbonate, (ii) sea surface temperature (SST), (iii) subsurface O_2 vertically integrated from 100 to 600 m, and (iv) net primary production (NPP) vertically integrated over the top 100 m. Our focus on subsurface O_2 concentrations is intended to characterize regimes ranging from oxygen minimum zones to the main thermocline of polar and circumpolar regions. Throughout the text that follows, we use Ω_{arag} to denote surface ocean Ω_{arag}.

2.2 Confidence intervals and detection of time of emergence

In order to quantify emergence characteristics, it is necessary to specify a timescale over which trends are calculated. We use decadal trends considered over 30 yr intervals on a gridpoint-by-gridpoint basis to quantify signal-to-noise ratios for each of the four ecosystem drivers. The signal is the trend obtained using the ensemble-mean, and the noise is the standard deviation of the 30 yr trends for the individual ensemble members. The signal-to-noise ratio is thereby calculated as the ratio of these two

BGD
11, 18189–18227, 2014

terms, and thereby associated with this specific timescale. The choice of a 30 yr trend window is motivated by the approximate length of relatively continuous elements of the global observing system and by the timescale of important natural variability events such as the Pacific Decadal Oscillation. Given that our model runs span 1950–2100, and our choice of 30 yr trends, signal-to-noise can effectively be calculated over each year spanning the period 1965–2085.

Central to our analysis is the model-derived quantification of confidence intervals for trend detection. We assume that the 30 yr trends for the 30 individual ensemble members are normally distributed. For a given time-window (30 years), the signal-to-noise ratio (SNR) is calculated using the relationship between the ensemble mean TREND and the standard deviation (σ_{noise}) of the trends of the various ensemble members, which we denote as NOISE:

$$\text{SNR} = \text{TREND}/\text{NOISE}. \quad (1)$$

Here we focus on a threshold of one for SNR, representing a confidence interval of 67 % for emergence. In other words, the threshold of one is used to characterize when the "signal" of anthropogenic climate change rises above the "noise" of natural background variability. However, the sensitivity to a choice of two (95 % confidence) for the threshold will also be considered. We choose two time intervals over which we consider average confidence intervals: the first is for the most recent decade 2005–2014, and the second is the decade 2075–2084 towards the end of the 21st century. The confidence intervals are calculated using 30 yr trends year-by-year over each of the 10 yr intervals before considering 10 yr averages over the respective intervals. An averaging interval of 10 yrs was sufficient to remove noise present in analysis for individual years in the confidence intervals, presumably due to the fact that even with 30 ensemble members the modes of variability aren't sufficiently randomized. Additionally, we also consider the sensitivity of the confidence intervals to the choice of the width of the trend window. To that end, confidence intervals will be presented for the case of a 10 yr window.

BGD
11, 18189–18227, 2014

Our analysis also includes diagnostics of Time of Emergence (ToE). In contrast to the confidence interval diagnostic for fixed time intervals, ToE requires that we first specify a fixed threshold (here we choose 67 %) for confidence intervals and then calculate the time (year) at which that is satisfied on a gridpoint-by-gridpoint basis for each ecosystem driver. For consistency, a 30 yr trend window is used here as well in the calculation of ToE.

3 Results

3.1 Temporal hierarchy of global and regional emergence of individual ecosystem drivers

We start the analysis with the temporal hierarchy of emergence for the globe as well as for various regions, such as the Southern Ocean (90–45° S), the southern subtropics (45–15° S), the equatorial band (15° S–15° N), the northern subtropics (15–45° N), and the subpolar and polar Northern Hemisphere (45–90° N) (Fig. 1). For each of the individual ecosystem drivers, the signal-to-noise ratio was calculated gridpoint-by-gridpoint, and then the area-weighted mean of this quantity were considered by region year-by-year (solid lines in Fig. 1). There is a distinct hierarchy in the emergence of the ecosystem drivers on a global scale (Fig. 1a), with Ω_{arag} (red line in Fig. 1a) already having risen above the one-standard deviation (67 %, black solid vertical axis in Fig. 1a) level by the beginning of the period considered (by 1965). This is followed by SST (green line in Fig. 1a), which globally emerges from the 67 % confidence level by the year 2000. O_2 inventories rising above the 67 % confidence interval by approximately 2060 (blue line in Fig. 1a), whereas NPP remains below the 67 % confidence level over the entire time period (purple line in Fig. 1a).

The regional behavior of the four ecosystem drivers is shown in Fig. 1b–f. Overall, the hierarchy found in the global analysis tends to be reproduced on a regional scale but with a few notable exceptions. First, the Southern Ocean differs from the other

BGD
11, 18189–18227, 2014

regions in that the O_2 inventories are more detectable than SST over the duration (blue solid line in Fig. 1b). Additionally, the subtropical SST tends to emerge from the 67 % confidence interval by 1990–2010 (green solid lines in Fig. 1c–e), with this not being the case for the Southern Ocean and the Northern subpolar/Arctic regions (green solid lines in Fig. 1b and f). The commonality is that the NPP signal remains below the 67 % confidence level for the entire duration in all regions, with the exception of the southern subtropics for the period post-2070.

3.2 Local emergence confidence intervals for individual ecosystem drivers

We next consider the spatial distributions of the confidence level that the signal (ensemble mean) in the four ecosystem drivers has emerged from the natural variability (standard deviation among the 30 ensemble members) for two different time periods: 2005–2014 (Fig. 2) and 2075–2084 (Fig. 3). For Ω_{arag} it is found that 99.8 % of the global domain exhibits the signal emerging above the noise with more than 67 % certainty (Fig. 2a). This indicates that observing platforms of 30 yr duration are able to detect trends nearly everywhere. The reasons for the early emergence is that changes in surface Ω_{arag} are mainly dictated by the increase in surface DIC, which closely follows atmospheric pCO_2 trends (e.g. Keller et al., 2014). For SST (Fig. 2b), 74.8 % of the global surface ocean has emerged with 67 % certainty from the noise. Especially the lower latitudes tend to have emerged with high confidence by 2005–2014, whereas the Southern Ocean south of 45° S and the northern subpolar and Arctic regions reveals only few confidence that they have emerged by 2005–2014. For O_2 inventories, 22.6 % of the global ocean has emerged with 67 % certainty from the noise (Fig. 2c). For NPP, only 14.8 % of the global ocean has emerged with 67 % certainty over 2005–2014 (Fig. 2d). Interestingly, the pattern for the O_2 inventories shown in Fig. 2c reveals emergence over important parts of the Pacific and Atlantic sectors of the Southern Ocean (defined as the region to the south of 45° S), in contrast to what is seen in SST. The lower latitudes reveal relatively little emergence by 2005–2014, but there are small areas within the subtropics of the North Pacific with emergence. For the case of NPP

BGD
11, 18189–18227, 2014

(Fig. 2d), there is very little evidence of emergence by 2005–2014 over most of the global domain, although the Equatorial Pacific Cold Tongue regions, parts of the Equatorial Atlantic, and the Agulhas regions show marginal emergence. This indicates that even with complete 30 yr time series for global NPP, it would not be possible in most regions to identify a significant trend.

Next we consider in Fig. 3 the confidence intervals calculated over 2075–2084. The patterns shown in Fig. 3 largely reinforce what was seen in Fig. 2, although clearly the emergent structures have expanded. Not surprisingly, Ω_{arag} (Fig. 3a) now stands emerged over 100 % of the global surface area with 67 % certainty at the end of the 21st century, consistent with what was shown over 2005–2014. For SST (Fig. 3b), 90.9 % of the global ocean has emerged with 67 % certainty, clearly having expanded beyond their limits from 2005–2014. This includes expansion into the North Atlantic, and the high latitudes over the Southern Ocean. For O_2 inventories (Fig. 3c), with 42.3 % of the globe emerged with 67 % certainty, the Southern Ocean increasingly emerges towards the end of the century, and the North Pacific subtropics have emerged with high confidence. For the case of NPP (Fig. 3d), with 23.7 % of the globe emerged with 67 % certainty, there continues to be only weak emergence over most of the globe, the exceptions being a coherent structure spanning the southern subtropics and subtropical front regions of the South Indian Ocean, the equatorial Pacific upwelling region, and then patchy regions over the Southern Ocean the eastern mid-latitude and subpolar North Atlantic.

Taken together, the results here indicate that the four ecosystem drivers are not advancing in unison with the same patterns and rates of their detectability over the globe. Ω_{arag} emerges first, consistent with what has been found in previous modeling studies (Friedrich et al., 2012), NPP emerges last, and then O_2 inventories and SST have their own contrasting patterns of emergence. Stated differently, random uncertainty associated with natural decadal variability poses significantly more important challenges for NPP than for Ω_{arag}, with O_2 inventories and SST falling between NPP and Ω_{arag}.

BGD
11, 18189–18227, 2014

3.3 Local emergence confidence intervals for the multiple ecosystem driver mean

We now consider a an average across the ecosystem drives of the confidence intervals for the same time intervals 2005–2014 (Fig. 4a) and 2075–2084 (Fig. 4b). To facilitate presentation and interpretation, we calculated averages within 14 biomes as defined by Henson et al. (2010). The biome definition separates the regions where phytoplankton growth is seasonally light limited (for mid- to high-latitudes), regions where the ocean is gaining heat (equatorial regions) and oligotrophic regions.

For the 2005–2014 period (Fig. 4a), the confidence intervals averaged across the four drivers have already risen above the threshold of one standard deviation (67 % confidence interval) in the Equatorial Atlantic, the South Atlantic, and the Arabian Sea. The Indian and Pacific sectors of the Southern Ocean weigh in at 60 % confidence intervals, thereby below one standard deviation. With the exception of the South Atlantic, subpolar regions are minimum regions for confidence intervals. For the case of the Equatorial Atlantic, where in fact O_2 inventories are increasing (Gnanadesikan et al., 2012; Cocco et al., 2013) (Fig. A1e), it is important to acknowledge that emergent O_2 inventories are thereby not to be understood as an ecosystem stressor, but in fact is better interpreted as a driver. Interestingly, the hemispheric asymmetry between the northern and southern subtropics of the Pacific is the reverse of the asymmetry found in the Atlantic.

By the later period 2075–2084 (Fig. 4b), the confidence intervals averaged over the four ecosystem drivers are higher than during the earlier period 2005–2014 except for the eastern equatorial Atlantic and the western equatorial Indian Oceans. There continues to be a hemispheric asymmetry between the subtropics of the northern and southern subtropical Pacific. Interestingly, the fact that subpolar regions have become maxima for the multiple ecosystem driver mean during the later period represents a reversal of what is found during the earlier period. For both hemispheres this reflects an important contribution from the O_2 inventories, as can be seen in the subpolar time se-

BGD
11, 18189–18227, 2014

ries changes in Fig. 1b and f. A relative decrease in variability in SST can be seen over the subpolar regions (Figs. A1d and A2d), contributing to the increased confidence in emergence over these regions (the differences between Figs. 2b and 3b).

As we did for the individual ecosystem drivers, we also consider here the fraction of the global area that has emerged for the multiple ecosystem driver mean over the periods 2005–2014 and 2075–2084. Following the procedure used in Figs. 2 and 3, a 30 yr trend window was used to characterize signal-to-noise over the respective time interval year-by-year. The result was then averaged over each of the ten-year time intervals gridpoint-by-gridpoint. Subsequently, area-weighted spatial averages were considered. For the earlier period (2005–2014), 40.9 % of the global ocean exhibits emergence with 67 % confidence. By 2075–2084, 62.5 % of the global ocean exhibits emergence with 67 % confidence.

Next we consider the emergence characteristics for the three ecosystem drivers with highest emergence confidence intervals (rather than all four drivers). This is shown for the time interval 2005–2014 in Fig. 4c, and for the time intervals 2075–2084 in Fig. 4d. For each case, the fields presented in Figs. 2 and 3 were considered gridpoint-by-gridpoint to find the three maximum amplitude ecosystem drivers, and these were then averaged over the same biome regions. Unsurprisingly, the confidence intervals are higher for this case with three largest ecosystem drivers than with all four. For the time interval 2005–2014, 87.8 % of the global surface area has emerged above the 67 % confidence interval (Fig. 4c), and for 2075–2084 98.8 % has emerged above 67 % (Fig. 4d).

We then consider averages over the dominant two ecosystem drivers for the period 2005–2014 (Fig. 4e) and 2075–2084 (Fig. 4f). Clearly the emergence characteristics are significantly higher here. As is revealed in the structures of locally maximum and minimum confidence intervals, the dominant influences over most of the global ocean are Ω_{arag} and SST in setting the even higher confidence intervals. For the time interval 2005–2014, 97.94 % of the global ocean is above the 67 % confidence interval. For the

BGD
11, 18189–18227, 2014

time interval 2075–2084, this has risen to 99.92 % of the global ocean having risen above the 67 % confidence interval.

Taken together, the six panels in Fig. 4 reveal a strong sensitivity to the number of ecosystem drivers used to characterize multiple ecosystem driver emergence. For the case of emergence over 2075–2084, it is interesting to note that the patterns are different. For four drivers, the Southern Ocean has the strongest emergence, whereas with two drivers the tropical band has the strongest emergence.

3.4 Sensitivity of confidence intervals to length of decadal trend window

Next we consider the sensitivity of our confidence interval calculation for the period 2005–2014 (Fig. 2) to the length of the window over which trends are calculated. The sensitivity of the confidence intervals over 2005–2014 to the width of the window is considered in Fig. 5, where a window of 10 yr has been used instead of the 30 yr used in Fig. 2. We show that for all four drivers, the choice of a 10 yr trend window results in important decreases in the confidence intervals over the global domain relative to a 30 yr trend window.

For Ω_{arag} (Fig. 5a), the confidence intervals are much lower in the regions directly impacted by El Niño variability with a 10 yr window than they are with a 30 yr window (Fig. 2a). Additionally, smaller confidence intervals are in evidence through the North Atlantic and parts of the Arctic, as well as in a well-defined band across the North Pacific. In fact, along much of both the west and east coasts of North America, confidence intervals are significantly lower than with the 30 yr window. This may have important implications in pointing to the need for sustained (multi-decadal) observing systems for ocean biogeochemistry in these regions.

For SST as well, the pattern obtained with a 10 yr window (Fig. 5b) reveals large differences from the pattern obtained with a 30 yr window (Fig. 2b). The relatively elevated values throughout much of the tropics and the subtropics have now disappeared, revealing relatively weak confidence intervals over global domain. A similar loss of confidence is found in for O_2 inventories (Fig. 5c) and for NPP (Fig. 5d). In fact for SST,

BGD
11, 18189–18227, 2014

O_2 inventories, and NPP, using a 10 yr window results in very weak confidence nearly everywhere over the global domain.

3.5 Time of emergence in individual and combined multiple ecosystem drivers

Next we consider Time of Emergence (ToE) in Fig. 6. Here, we use a one standard deviation threshold to define ToE, and our intention is to represent another dimension to the emergence question, namely that of time. A 10 year tolerance window with a robust Loess filter has been applied for the fields in Fig. 6, as described in Appendix B. First we consider Ω_{arag} (Fig. 6a), with this revealing that most of the emergence has already occurred by the start of the analysis period (before 1965), consistent with what was seen in the confidence interval analysis. The only exceptions are relatively high dynamical variability zone within the equatorial Pacific, and certain high variability structures associated with western boundary current regions. For SST (Fig. 6b), the ToE is within the 20th century for much of the tropics, with a tendency for this ToE to shift to the 21st century for much of the subtropical and subpolar regions. For much of the high-latitude Southern Ocean region, there is no emergence during the analysis period (before 2085). This is also true for important sectors of the northern North Atlantic. For O_2 inventories (Fig. 6c) an early ToE is evident for the Southern Ocean as well as the eastern equatorial Atlantic, largely consistent with what was seen in Fig. 2. Alternating zonal structures of early and late ToE are seen in the Equatorial Pacific, and a patchwork of structures with very different ToE is in evidence over much of the ocean away from the Southern Ocean. In fact, the patchwork-like structures are in even stronger evidence for NPP (Fig. 6d). Consistent with what was seen in Fig. 2d, relatively early ToE is in evidence for both the Agulhas and the Equatorial Pacific Cold Tongue regions. Otherwise there are alternating bands of saturation for both early (pre-1965) and late (post-2085) ToE. The adjacent early and late saturation regions are the consequence of choosing a threshold for ToE. Thus the boundaries between such regions may not in general be reflecting real biome structures in the model domain. This is addressed in more detail in the Appendix (Figs. A3 and A4).

BGD
11, 18189–18227, 2014

4 Discussion and conclusions

We set out to evaluate the emergence characteristics of four ecosystem drivers (surface Ω_{arag}, SST, subsurface O_2, and NPP) of marine ecosystems, with two questions driving this investigation. The first motivation stems from an interest in identifying when the secular trend in drivers becomes evident or perceptible for local marine ecosystems relative to the natural background decadal variability to which the organisms have adapted. The second pertains to the optimization of the ocean biogeochemical observing system, and the application of models to advance this optimization through iterative communication with the community of researchers evaluating network design. Building on the previous work of Frölicher et al. (2009), this was pursued using a suite of large initial-condition ensemble simulations, as it is only with this approach that one can infer the secular trend (ensemble mean) for a model by filtering natural variability through an averaging procedure. The averaging procedure operates on not only patterns of climate modes such as ENSO (Wittenberg et al., 2014), but also on natural variability on smaller scales associated with variations in gyre boundaries that are not correlated to climate modes. Importantly, with this large ensemble approach, one does not need to assume that variability in the system is stationary in time.

Our main result is that there is a temporal hierarchy in the emergence of the four ocean ecosystem drivers above the level of background natural variability. This is strongly evident in Fig. 1. Ω_{arag} emerges earliest, NPP emerges latest, and both O_2 inventories and SST fall between the two. Additionally, three (SST, O_2 inventories, and NPP) of the four drivers considered here exhibit large regions where detection of secular trends is significantly complicated by the presence of natural decadal variability in the climate system. Our results also revealed very pronounced differences in the patterns for the confidence intervals for the emergence of SST and O_2 inventories (Fig. 2). For SST, the Southern Ocean emerges relatively late (post-2014) and the tropics emerge rather early (pre-2014), in line with earlier studies (Mora et al., 2013). For O_2 inventories, on the other hand, the Pacific and Atlantic sectors of the Southern

BGD
11, 18189–18227, 2014

Ocean exhibit regions of relatively early emergence (pre-2014) and the tropics emerge rather late (post-2014). The coalescence of the different global ecosystem drivers in certain regions is already creating a number of hot-spots (Fig. 4), with the Southern Ocean and more generally the high latitudes projected to increase in importance by 2075–2084.

Consistent results regarding the temporal hierarchy of ecosystem driver emergence were found through the analysis of confidence intervals (Figs. 2 and 3) and time of emergence (ToE) (Fig. 6) as diagnostics. However, we prefer the confidence interval analysis over the ToE analysis for two reasons. First, for the four ecosystem drivers the saturation characteristics of the ToE analysis (emergence before 1965 or after 2085) are widespread, complicating interpretation. Second, and perhaps more importantly, ToE diagnostics require a specification of a threshold of signal-to-noise that is somewhat arbitrary (here we have considered both 1 and 2 standard deviations, but have chosen to emphasize the less conservative value of 1 in Fig. 6).

The quantification of signal-to-noise at the center of our analysis relies on joint use of a suite of Large Initial-Condition Ensemble Simulations using an individual Earth System Model (GFDL's ESM2M). However, previously published analyses indicate that the collection of Earth System Models developed by different modeling centers exhibit disparate amplitudes for the secular trends in individual ecosystem drivers or stressors (Bopp et al., 2013). For example, different ESMs are likely to differ more in their projected changes in NPP than they are in Ω_{arag} or SST, since at least with Ω_{arag} or SST the ESMs are largely consistent in the sign of their response (Bopp et al., 2013; Steinacher et al., 2010; Cocco et al., 2013). In high latitudes, ESMs are generally consistent in simulating decreasing ocean O_2 inventories under 21st century climate change (Cocco et al., 2013). However, it is worth noting that in GFDL ESM2M NPP changes by only 2 % under the historical/RCP8.5 scenario, whereas NPP tends to decrease by approximately 10 % for a multi-model of CMIP5 ESMs under the same scenario (C. Laufkötter, personal communication, 2014). Additionally, different earth system models exhibit different noise or underlying natural variability characteristics

BGD
11, 18189–18227, 2014

for individual ecosystem drivers or stressors (Keller et al., 2014). Such inter-model differences strongly suggest that the temporal and spatial characteristics of emergence should be model-dependent, as has been shown for the case of surface air temperature by Hawkins and Sutton (2011). Alternative emissions scenarios may also lead to changes in both the signal and the noise. Investigations of the sensitivity of our results to alternative scenarios for anthropogenic emissions and other model projections may be subject to further studies.

Our results also point to the importance of maintaining a sustained multi-decadal observing system for ocean biogeochemistry and ecosystem drivers. For the four drivers considered here, the confidence intervals found with a 30 yr window for calculating trends (Fig. 2) are significantly higher than those found with a 10 yr window (Fig. 5). For the case with a 10 yr window, even Ω_{arag} reveals expanses of non-emergence over the recent decade (2005–2014). One is motivated for the sake of argument to consider that a perfectly resolving (all time and space scales) ocean biogeochemistry system is in place, thereby providing the community with a perfectly resolved global time-varying state estimate for the drivers considered here. The results presented here indicate that a state estimate of several decades may well be required to characterize emergence characteristics for multiple ecosystem drivers with reasonable confidence. Of course the global observing system will always be imperfect, and this fact will only increase the duration of sustained measurements needed to provide a satisfactory accounting of emergence.

There is not yet a scientific consensus on the impact individual ecosystem drivers will have on ocean organisms and ecosystems, much less the combined effects of multiple drivers acting in concert. It is currently unknown if the combined effects are antagonistic or synergistic as opposed to simply additive. To date resource management strategies have tended to focus on the impact of individual drivers, with little consideration or attention devoted to potential relationships and feedbacks between the drivers. What is clear, however, is that anthropogenic CO_2 emissions to the atmosphere are more generally the common "driver" investigated here, and at the very least individually the

BGD
11, 18189–18227, 2014

model suggest that the individual ecosystem drivers all exhibit temporal and spatial scales over which their secular trend rises above the level to which marine species are accustomed through natural variability. This single driver underscores the necessity of a single policy response (reduction in emissions). Substantial mitigation measures are required if ocean ecosystems are to be spared from the "quadruple whammy" of the ecosystem drivers considered here.

Appendix A: Secular trends and natural variability underlying signal-to-noise analysis

We characterize here the secular trends (left columns in Figs. A1 and A2; referred below as TREND) and standard deviations of the secular trends (right columns in Figs. A1 and A2; referred below as NOISE) separately. Recall that the signal-to-noise ratio is defined as the ratio of these two fields. Ω_{arag} decreases everywhere over the global domain (Fig. A1a), with minimum relative rates of decrease in the equatorial regions, and a general tendency towards stronger relative rates of decrease at high latitudes. Largest NOISE of Ω_{arag} is simulated in a number of dynamically active regions, including the margins of the subtropical gyres and the equatorial Pacific. However, with the exception of a few isolated regions, the TREND is everywhere significantly larger than the NOISE for Ω_{arag}. For SST, the TREND over 2005–2014 is positive (warming) over most of the globe, with the notable exception of the western subpolar North Atlantic and large expanses of the Southern Ocean (cooling). This stands in contrast to Ω_{arag}, where the trend had the same sign over the entire domain.

The NOISE for SST finds largest expression in the subpolar regions of the Northern Hemisphere and over parts of the Southern Ocean. In fact it can be seen in the Fig. 1c and d that the extratropical regions of weak or negative TREND in SST are associated with enhanced variability. The tropics, on the other hand, reveal only modest NOISE amplitude relative to the TREND. Taken together, this helps to account for the fact that the confidence interval map in Fig. 2b reveals high confidence in the tropics relative

BGD
11, 18189–18227, 2014

to the subpolar regions. As has been stated in the main text, it may seem somewhat surprising that the signal-to-noise-ratio is relatively elevated in the Equatorial Pacific, given that this is the region of largest natural variability in the climate system. It is important to emphasize here that we are considering trends over a 30 yr interval in our quantification of NOISE rather than considering the standard deviation associated with interannual variability for each of the ecosystem drivers.

For the case of O_2 inventories, a decreasing TREND can be seen in the well-ventilated thermocline of the high latitudes. Within the tropics and subtropics, structures of positive trend do occur. As with SST but in contrast with Ω_{arag}, the sign of the ensemble-mean response of O_2 inventories is not of the same sign everywhere. However, there are also pronounced structures of larger NOISE in O_2 inventories, which over many regions are associated with decadal variations in gyre boundaries and frontal regions. The most prominent extended region where the TREND is larger than the NOISE is over a broad expanse of the Pacific and Atlantic sectors of the Southern Ocean (as seen in Fig. 2c).

For the case of Net Primary Productivity (NPP), both the TREND and the NOISE patterns show relatively narrowly-defined but large-amplitude structures. There is a trend in the zonal gradient in NPP across the equatorial Pacific, as well as a trend towards enhanced NPP along the poleward flanks of the Southern Hemisphere subtropical gyres. For the NOISE, a series of relatively narrow structures of high amplitude are found winding through the tropics. Over most regions of the globe, the NOISE is of sufficient amplitude relative to TREND to give the consistently lowest Confidence Interval distribution of the four ecosystem drivers considered here (Fig. 2d).

It is worth noting in Fig. A1 that the unforced components (right column) of the four drivers exhibit large-scale spatial coherence rather than small grid-scale noise. However, these structures are distinct for each of the drivers.

The same fields for the time interval 2075–2084 are considered in Fig. A2. The amplitudes in TRENDS have increased in general, but important elements of the TREND structures are similar as for the earlier period. The structures of the NOISE are quite

BGD
11, 18189–18227, 2014

similar to those found for the equivalent drivers during the earlier period. However, the amplitude of the variations is in many cases different for 2075–2084 than for 2005–2014. This indicates that the amplitude of the background natural variability is not stationary. For the case of SST and O_2, the standard deviation of natural decadal variations decreases over the Southern Ocean.

Appendix B: Temporal filtering and trend detection

The task of calculating Time of Emergence (ToE) in Fig. 6 is complicated by the fact that the signal-to-noise ratio (SNR) in time series for individual grid points in the ocean model does not in general tend to be monotonically increasing over the period 1950–2100. Rather, the evolution of the SNR can reflect that for this particular diagnostic, the 30 ensemble members may not be sufficient to eliminate noise when averaged.

As an illustration of this problem, we consider in Fig. A3 the evolution of the SNR for sea surface temperature a region in the Pacific sector of the Southern Ocean bounded by 130–100° W and 45–60° S. The time series of the SNR for the various points in this region are superposed in Fig. A3a. The non-monotonic nature of the increase in SNR through time is evident. With this unfiltered SNR calculated directly from the annual mean model output, there are relatively short-timescale excursions above the two standard deviation threshold that precede by a number of decades the more permanent crossing of the one standard deviation threshold. However, this does not occur for all of the grid points in the domain of interest. As a consequence of these early excursions above the one standard deviation threshold, the spatial pattern of ToE using a strict definition of first crossing (Fig. A3b) reveals a spatial pattern that has a ToE before 2014 (present time) over more than 50 % of the region.

It is important to understand the degree to which the ToE structure in Fig. A3b reflects short-term vs. longer-term or permanent transitions of the SNR about the one standard deviation threshold, rather than short-term excursions. To evaluate this, we apply to the full suite of time series shown in Fig. A3a (gridpoint-by-gridpoint SNR for SST) a robust

BGD
11, 18189–18227, 2014

Loess filter. We have chosen to use a 10 yr tolerance window with the robust Loess filter, with this serving effectively as a low-pass filter that is obtained using ten-year local regressions over the entire time period for each individual gridpoint. The result of applying the robust Loess filter is shown in Fig. A4a, where the filtered time series are shown as red lines overlaying the full time series shown in blue. The filtered time series are seen to behave as low-pass filters that effectively remove the higher frequency components. When these smoothed time series are used to define ToE with the same two standard deviation threshold, the resulting pattern (Fig. A4b) reveals important differences relative to the unfiltered time series. The structures with post-2014 ToE now occupy most of the domain. This indicates the strong sensitivity of the spatial pattern of ToE to the time-filtering of the SNR time series.

The sensitivity of the Time of Emergence (ToE) to the width of the window used for calculating trends is considered in Fig. A5. Here the window is chosen to be 10 yrs, and this result is to be contrasted to what was found for ToE using a 30 yr window as considered in Fig. 6. Clearly the narrower trend interval of 10 yrs results in saturation (post-2095 emergence for this case of a 10 yr trend window) on nearly global scales for all of the ecosystem drivers except for Ω_{arag}. This indicates a strong sensitivity of ToE to the timescale chosen for the analysis, consistent with what was shown in Fig. 4 for the confidence interval sensitivity analysis. Fig. A5 is valuable in that the strong saturation characteristics for three of the drivers (post-2085 emergence) are much more difficult to interpret than the parallel and favored analysis with confidence intervals.

We also consider the sensitivity of the Time of Emergence (ToE) to the width of the tolerance window used for the robust Loess filter in Fig. A6a. For each case, the sensitivity of the ToE to the width of the tolerance window (described above) is considered for each of the four ecosystem drivers. For each case, the area-weighted global mean sensitivity is considered. The sensitivity is weak for Ω_{arag}, with the dynamic range of the sensitivity being only a few years as the tolerance window is modified from 5 to 25 yr. The sensitivity is largest for O_2 inventories, with a decrease of the ToE of 80 years as one transitions from a 5 to a 25 yr tolerance window. This strong sensitivity is likely the

BGD
11, 18189–18227, 2014

expression of the red spectrum of modes of variability in thermocline depth impacting O_2 inventories in their temporal variability. The sensitivities of SST and NPP are quite similar, both being approximately 50 % of the amplitude of the sensitivity seen for O_2 inventories. In fact, the sensitivity of NPP should be expected to be larger than that of SST, given that the sensitivity shown here may be obscured by the saturation characteristics of NPP.

We also consider in Fig. A6b the sensitivity of the ToE to the choice of a SNR ratio of one in Fig. 6. Here as well, the sensitivity considers the global area-weighted mean. The sensitivity is strongest for SST, and then the second strongest is found for O_2 inventories. The sensitivity is weakest or Ω_{arag} and for NPP, but as a caveat it needs to be emphasized that both of these fields exhibit saturation behavior in Fig. 6. If the suite of 30 ensemble runs with ESM2M had been runs for a significantly longer time intervals, say from 1860–2300, then one would expect that the sensitivity for these two fields to be more pronounced.

Acknowledgements. The contribution of K. B. Rodgers came through awards NA17RJ2612 and NA08OAR4320752, which includes support through the NOAA Office of Climate Observations (OCO). The statements, findings, conclusions, and recommendations are those of the authors and do not necessarily reflect the views of NOAA or the U.S. Department of Commerce. T. L. Frölicher acknowledges financial support from the SNSF (Ambizione grant PZ00P2_142573). J. Lin's work in a summer internship was supported through the Princeton Environmental Institute (PEI). The authors would like to thank John Dunne at GFDL for his contributions with model development and for access to computing resources.

References

Anderson, J. L., Balaji, V., Broccoli, A. J., Cooke, W. F., Delworth, T. L., Dixon, K. W., Donner, L. J., Dunne, K. A., Freidenreich, S. M., Garner, S. T., Gudgel, R. G., Gordon, C. T., Held, I. M., Hemler, R. S., Horowitz, L. W., Klein, S. A., Knutson, T. R., Kushner, P. J., Langenhost, A. R., Lau, N.-C., Liang, Z., Malyshev, S. L., Milly, P. C. D., Nath, M. J., Ploshay, J. J., Ramaswamy, V., Schwarzkopf, M. D., Shevliakova, E., Sirutis, J. J., Soden, B. J., Stern, W. F.,

BGD
11, 18189–18227, 2014

Thompson, L. A., Wilson, R. J., Wittenberg, A. T., and Wyman, B. L.: The new GFDL global atmosphere and land model AM2-LM2: evaluation with prescribed SST simulations, J. Climate, 17, 4641–4673, 2004.

Bopp, L., Monfray, P., Aumont, O., Dufresne, J. L., Le Treut, H., Madec, G., Terray, L., and Orr, J. C.: Potential impact of climate change on marine export production, Global Biogeochem. Cy., 15, 81–99, 2001.

Bopp, L., Resplandy, L., Orr, J. C., Doney, S. C., Dunne, J. P., Gehlen, M., Halloran, P., Heinze, C., Ilyina, T., Séférian, R., Tjiputra, J., and Vichi, M.: Multiple stressors of ocean ecosystems in the 21st century: projections with CMIP5 models, Biogeosciences, 10, 6225–6245, doi:10.5194/bg-10-6225-2013, 2013.

Cocco, V., Joos, F., Steinacher, M., Frölicher, T. L., Bopp, L., Dunne, J., Gehlen, M., Heinze, C., Orr, J., Oschlies, A., Schneider, B., Segschneider, J., and Tjiputra, J.: Oxygen and indicators of stress for marine life in multi-model global warming projections, Biogeosciences, 10, 1849–1868, doi:10.5194/bg-10-1849-2013, 2013.

Delworth, T. L., Broccoli, A. J., Rosati, A., Stouffer, R. J., Balaji, V., Beesley, J. A., Cooke, W. F., Dixon, K. W., Dunne, J., Dunne, K. A., Durachta, J. W., Findell, K. L., Ginoux, P., Gnanadesikan, A., Gordon, C. T., Griffies, S. M., Gudgel, R., Harrison, M. J., Held, I. M., Hemler, R. S., Horowitz, L. W., Klein, S. A., Knutson, T. R., Kushner, P. J., Langenhorst, A. R., Lee, H.-C., Lin, S.-J., Lu, J., Malyshev, S. L., Milly, P. C. D., Ramaswamy, V., Russell, J., Schwarzkopf, M. D., Shevliakova, E., Sirutis, J. J., Spelman, M. J., Stern, W. F., Winton, M., Wittenberg, A. T., Wyman, B., Zeng, F., and Zhang, R.: GFDL's CM2 global coupled climate models. Part I: Formulation and simulation characteristics, J. Climate, 19, 643–674, 2006.

Deser, C., Phillips, A. S., Alexander, M. A., and Smoliak, B. V.: Projecting North American climate over the next 50 years: uncertainty due to internal variability, J. Climate, 27, 2271–2296, 2014.

Diffenbaugh, N. S. and Scherer, M.: Observational and model evidence of global emergence of permanent, unprecedented heat in the 20th and 21st centuries, Clim. Change, 107, 615–624, 2011.

Doney, S. C., Fabry, V. J., Feely, R. A., and Kleypas, J. A.: Ocean acidification: the other CO_2 problem, Annu. Rev. Mar. Sci., 1, 169–192, 2009.

Doney, S. C., Ruckelshaus, M., Duffy, J. E., Barry, J. P., Chan, F., English, C. A., Galindo, H. M., Grebmeier, J. M., Hollowed, A. B., Knowlton, N., Polovina, J., Rabalais, N. N., Syde-

BGD
11, 18189–18227, 2014

man, W. J., and Talley, L. D.: Climate change impacts on marine ecosystems, Annu. Rev. Mar. Sci., 4, 11–37, 2012.

Dunne, J. P., Gnanadesikan, A., Sarmiento, J. L., and Slater, R. D.: Technical description of the prototype version (v0) of Tracers of Phytoplankton with Allometric Zooplankton (TOPAZ) ocean biogeochemical model as used in the Princeton IFMIP model, Biogeosciences, 7 (Suppl.), 3593, doi:10.4195/bg-7-3593-2010, 2010.

Dunne, J. P., John, J. G., Adcroft, A. J., Griffies, S. M., Hallberg, R. W., Shevliakova, E., Stouffer, R. J., Cooke, W., Dunne, K. A., Harrison, M. J., Krasting, J. P., Halyshev, S. L., Milly, P. C. D., Phillipps, P. J., Sentman, L. T., Samuels, B. L., Spelman, M. J., Winton, M., Wittenberg, A. T., and Zadeh, N.: GFDL's ESM2 global coupled climate-carbon earth system models. Part I: Physical formulation and baseline simulation characteristics, J. Climate, 25, 6646–6665, 2012.

Dunne, J. P., John, J. G., Shevliakova, E., Stouffer, R. J., Krasting, J. P., Malyshev, S. L., Milly, P. C. D., Sentman, L. T., Adcroft, A. J., Cooke, W., Dunne, K. A., Griffies, S. M., Hallberg, R. W., Harrison, M. J., Levy, H., Wittenberg, A. T., Phillips, P. J., and Zadeh, N.: GFDL's ESM2 global coupled climate-carbon earth system models. Part II: Carbon system formulation and baseline simulation characteristics, 26, 2247–2267, 2013.

Emerson, S., Watanabe, Y., Ono, T., and Mecking, S.:Temporal trends in apparent oxygen utilization in the upper pycnocline of the North Pacific: 1980–2000, J. Oceanogr., 60, 139–147, 2004.

Friedlingstein, P., Andrew, R. M., Rogelj, J., Peters, G. P., Canadell, J. G., Knutti, R., Luderer, G., Raupach, M. R., Schaeffer, M., van Vuuren, D. P., and Le Quéré, C.: Persistent growth of CO_2 emissions and implications for reaching climate targets, Nat. Geosci., 7, 709–715, 2014.

Friedrich, T., Timmermann, A., Abe-Ouchi, A., Bates, N. R., Chikamoto, M. O., Church, M. J., Dore, J. E., Gledhill, D. K., Gonzalez-Davila, M., Henemann, M., Ilyina, T., Jungclaus, J. H., McLeod, E., Mouchet, A., and Santana-Casiano, J. M.: Detecting regional anthropogenic trends in ocean acidification against natural variability, Nature Climate Change, 2, doi:10.1038/nclimate1372, 2012.

Frölicher, T. L., Joos, F., Plattner, G. K., Steinacher, M., and Doney, S. C.: Natural variability and anthropogenic trends in oceanic oxygen in a coupled carbon cycle-climate model ensemble, Global Biogeochem. Cy., 23, GB1003, doi:10.1029/2008GB003316, 2009.

BGD
11, 18189–18227, 2014

Gnanadesikan, A., Dunne, J. P., and John, J.: Understanding why the volume of suboxic waters does not increase over centuries of global warming in an Earth System Model, Biogeosciences, 9, 1159–1172, doi:10.5194/bg-9-1159-2012, 2012.
Griffies, S. M.: Elements of MOM4p1. GFDL Ocean Group Tech. Rep. 6, 37 pp., available at: http://data1.gfdl.noaa.gov/~arl/pubrel/o/old/doc/mom4p1_guide.pdf(last access: 2010), 2009.
Gruber, N.: Warming up, turning sour, losing breath: ocean biogeochemistry under global change, Phil. Trans. R. Soc. A, 369, 1980–1996, 2011.
Hall, J., Diaz, R. J., Gruber, N., and Wilhelmsson., D.: Managing ocean environments in a changing sustainability and economic, in: Managing Ocean Environments in a Changing Climate, edited by: Noone, K. J., Sumaila, U. S., and Diaz, R. J., Elsevier Inc., Burlington, MA, 193–222, 2013.
Hawkins, E. and Sutton, R.: The potential to narrow uncertainty in projections of regional precipitation change, Clim. Dynam., 37, 407–418, 2011.
Hawkins, E. and Sutton, R.: Time of emergence of climate signals, Geophys. Res. Lett., 39, L01702, doi:10.1029/2011GL050087, 2012.
Henson, S. A.: Slow science: the value of long ocean biogeochemistry records, Philos. T. R. Soc. A, 372, 20130334, doi:10.1098/rsta.2013.0334, 2014.
Henson, S. A., Sarmiento, J. L., Dunne, J. P., Bopp, L., Lima, I., Doney, S. C., John, J., and Beaulieu, C.: Detection of anthropogenic climate change in satellite records of ocean chlorophyll and productivity, Biogeosciences, 7, 621–640, doi:10.5194/bg-7-621-2010, 2010.
Keeling, R. F., Koertzinger, A., and Gruber, N.: Ocean deoxygenation in a warming world, Annu. Rev. Mar. Sci., 2, 199–229, 2010.
Keller, K. M., Joos, F., and Raible, C. C.: Time of emergence of trends in ocean biogeochemistry, Biogeosciences, 11, 3647–3659, doi:10.5194/bg-11-3647-2014, 2014.
Kouketsu, S., Fukasawa, M., Sasano, D., Kumamoto, Y., Kawano, T., Uchida, H., and Doi., T.: Changes in water properties around North Pacific intermediate water between the 1980s, 1990s and 2000s, Deep-Sea Research II, 57, 1177–1187, 2010.
Lyu, K., Zhang, X., Church, J. A., Slangen, A. B. A., and Hu, J.: Time of emergence for regional sea-level change, Nature Climate Change, 4, 1006–1010, doi:10.1038/nclimate2397, 2014.
Mahlstein, I., Hegerl, G., and Solomon, S.: Emerging local warming signals in observational data, Geophys. Res. Lett., 39, L21711, doi:10.1029/2012GL053952, 2012.

BGD
11, 18189–18227, 2014

Martinez, E., Antoine, D., d'Ortenzio, F., and Gentili, B.: Climate-driven basin-scale decadal oscillations of oceanic phytoplankton, Science, 326, 1253–1256, 2009.
Mecking, S., Langdon, C., Feely, R. A., Sabine, C. L., Deutsch, C. A., and Min, D.-H.: Climate variability in the North Pacific thermocline diagnosed from oxygen measurements: an update based on the U. S. CLIVAR/CO_2 Repeat Hydrography cruises, Global Biogeochem. Cy., 22, GB3015, doi:10.1029/2007GB003101, 2008.
Mora, C., Frazier, A. G., Longman, R. J., Dacks, R. S., Walton, M. M., Tong, E. J., Sanchez, J. J., Kaiser, L. R., Stender, Y. O., Anderson, J. M., Ambrosino, C. M., Fernandez-Silva, I., Giuseffi, L. F., and Giambelluca, T. W.: The projected timing of climate departure from recent variability, Nature, 502, 183–187, 2013.
Rodgers, K. B., Key, R. M., Gnanadesikan, A., Sarmiento, J. L., Aumont, O., Bopp, L., Doney, S. C., Dunne, J. P., Glover, D. M., Ishida, A., Ishii, M., Jacobson, A. R., Lo Monaco, C., Maier-Reimer, E., Mercier, H., Metzl, N., Pérez, F. F., Rios, A. F., Wanninkhof, R., Wetzel, P., Winn, C. D., and Yamanaka, Y.: Using altimetry to help explain patchy changes in hydrographic carbon measurements, J. Geophys. Res., 114, C09013, doi:10.1029/2008JC005183, 2009.
Sarmiento, J. L., Hughes, T. M. C., Stouffer, R. J., Manabe, S.: Simulated response of the ocean carbon cycle to anthropogenic climate warming, Nature, 393, 245–249, 1998.
Steinacher, M., Joos, F., Frölicher, T. L., Bopp, L., Cadule, P., Cocco, V., Doney, S. C., Gehlen, M., Lindsay, K., Moore, J. K., Schneider, B., and Segschneider, J.: Projected 21st century decrease in marine productivity: a multi-model analysis, Biogeosciences, 7, 979–1005, doi:10.5194/bg-7-979-2010, 2010.
Takatani, Y., Sasano, D., Nakano, T., Midorikawa, T., and Ishii, M: Decrease of dissolved oxygen after the mid-1980s in the western North Pacific subtropical gyre along the 137° E repeat section, Global Biogeochem. Cy., 26, GB2013, doi:10.1029/2011GB004227, 2012.
Timmermann, A., Oberhuber, J., Bacher, A., Esch, M., Latif, M., and Roeckner, E.: Increased El Niño frequency in a climate model forced by future greenhouse warming, Nature, 298, 694–697, 1999.
van Vuuren, D. P., Edmonds, J., Kainuma, M., Riahi, K., Thomson, A., Hibbard, K., Hurtt, G., Kram, T., Krey, V., Lamarque, J.-F., Masui, T., Meinhausen, M., Nakicenovic, N., Smith, S. J., and Rose, S. K.: The representative concentration pathways: an overview, Clim. Change, 109, 5031, doi:10.1007/s10584-011-0148-z, 2011.

BGD
11, 18189–18227, 2014

Wittenberg, A. T., Rosati, A., Delworth, T. L., Vecchi, G. A., and Zeng, F.: ENSO modulations: is it decadally predictable?, J. Climate, 27, 2667–2681, 2014.
Zhang, Y., Wallace, J. M., and Battisti, D. S.: ENSO-like interdecadal variability: 1900–93, J. Climate, 10, 1004–1020, 1997.

BGD
11, 18189–18227, 2014

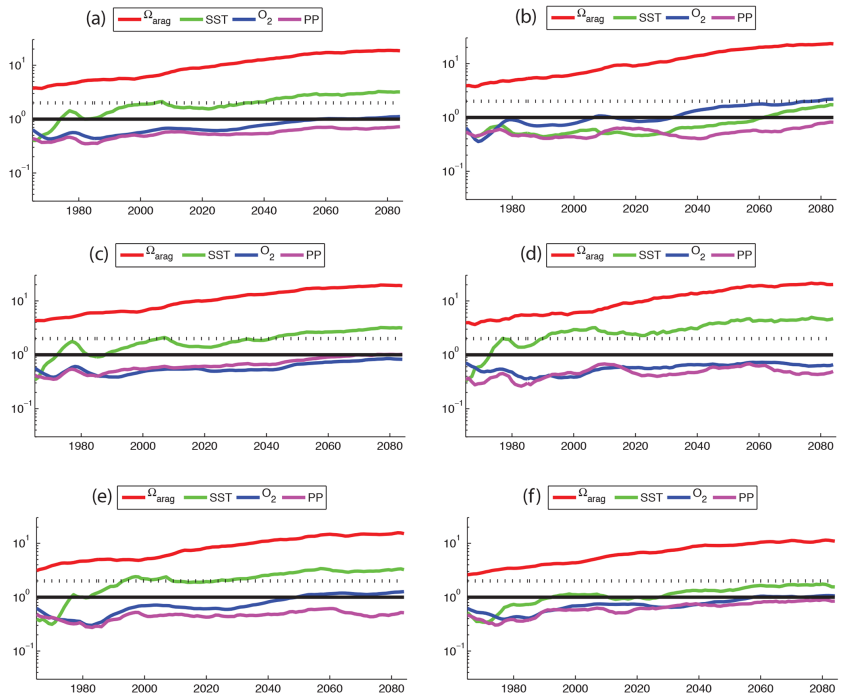

Figure 1. Time series of (area weighted) averages of signal-to-noise ratio (SNR) for four marine ecosystem drivers, considered over a number of ocean regions: **(a)** global, **(b)** 90–45° S, **(c)** 45–15° S, **(d)** 15–15° N, **(e)** 15–45° N, and **(f)** 45–90° N. The four drivers are Ω_{arag}, SST, O_2 inventories, and NPP. The SNR has been calculated individually for each driver on a gridpoint-by-gridpoint basis using a 30 yr trend window. The vertical axis has a logarithmic scale (non-dimensional) representing standard deviations. The 1-standard deviation threshold is shown as a solid horizontal line, and the 2-standard deviation threshold is shown as a dashed line in each panel.

BGD
11, 18189–18227, 2014

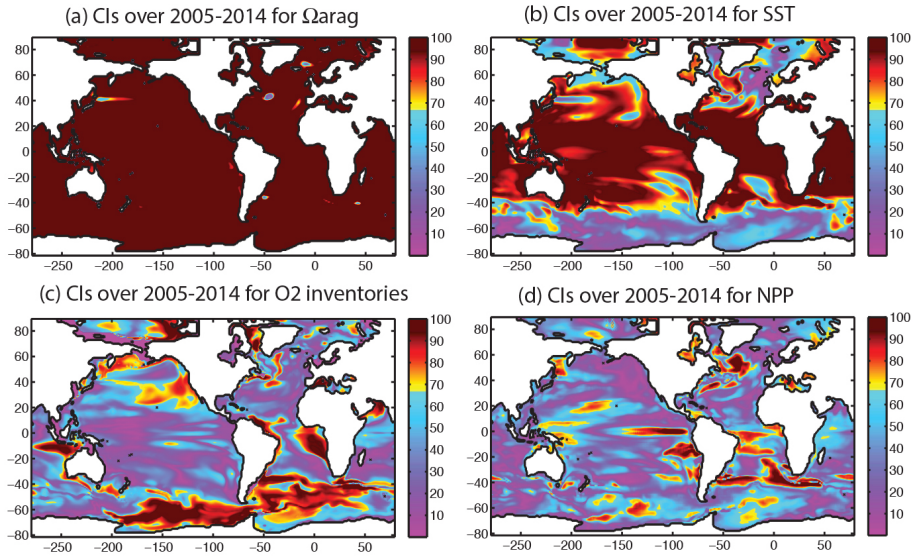

Figure 2. Confidence interval maps averaged over 2005–2014 for **(a)** Ω_{arag}, **(b)** SST, **(c)** O_2 inventories, and **(d)** NPP. For the case of O_2 inventories in panel **(c)**, shelf regions where the ocean depth is less than 600 m deep are not included in the analysis, and identified with black shading. For each case, a 30 yr window has been used to calculated trends gridpoint-by-gridpoint for each year between 2005 and 2014. An average over 10 years was considered to remove shorter timescale fluctuations in the signal-to-noise ratio. Note that the color scheme here is chosen such that saturation occurs (maroon color) above the 67 % confidence interval. Warm colors indicate confidence intervals ranging from 67–95 % (one to two standard deviations), and cool colors span the range 0–67 % (less than one SD).

BGD
11, 18189–18227, 2014

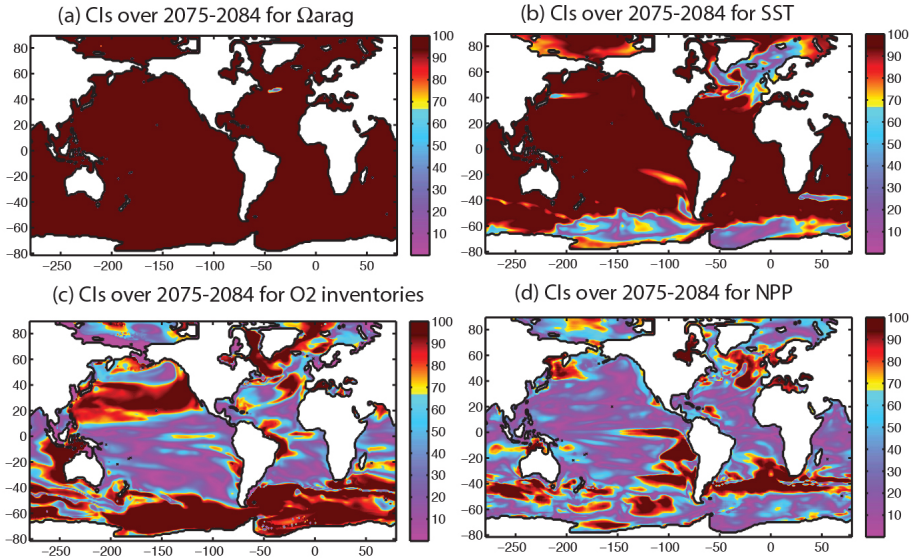

Figure 3. Same as Fig. 2, but averaged over the 2075–2084 period.

BGD
11, 18189–18227, 2014

Emergence of multiple ocean ecosystem drivers in a large ensemble suite

K. B. Rodgers et al.

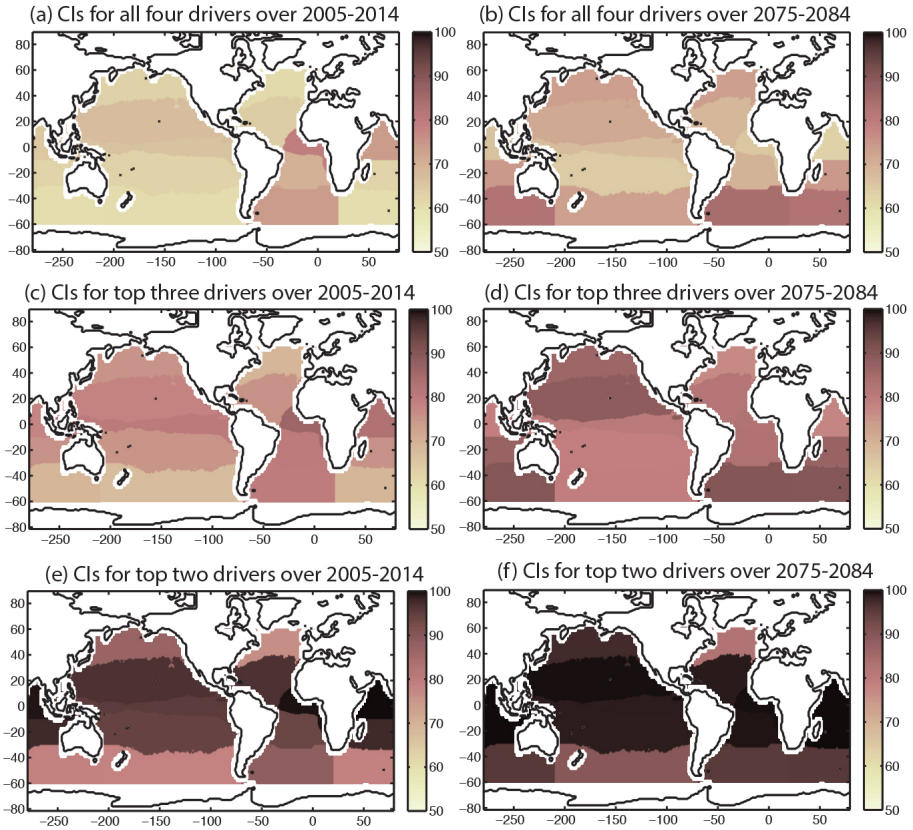

Figure 4. Confidence intervals for two ten-year intervals, namely 2005–2014 (left column), and 2075–2084 (right column). The confidence intervals for **(a)** the four ecosystem drivers (Ω_{arag}, SST, O_2 inventories, and NPP) over 2005–2014 are taken as the average over the fields shown in Fig. 2, and **(b)** the confidence intervals shown for the four drivers over 2075–2084 are taken as the average of the fields shown in Fig. 3.

BGD
11, 18189–18227, 2014

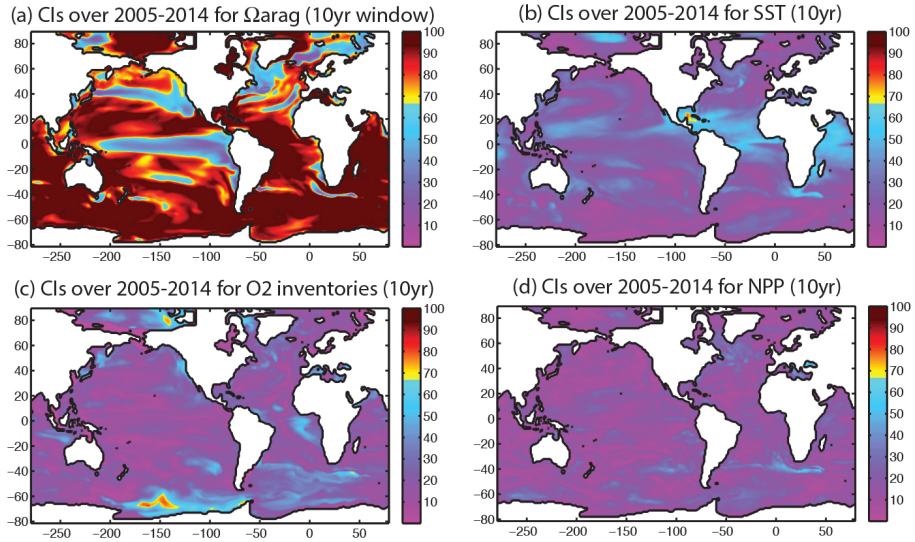

Figure 5. The confidence intervals for emergence of each of the ecosystem drivers for the time period 2005–2014, using a 10 yr window for calculating trends. The analysis here is otherwise identical to that shown in Fig. 2, except that there a 30 yr window was chosen. The panels show the distributions for **(a)** Ω_{arag}, **(b)** SST, **(c)** O_2 inventories, and **(d)** NPP. This analysis reveals significantly lower confidence intervals for the 10 yr window than for the 30 yr window for each of the drivers.

BGD
11, 18189–18227, 2014

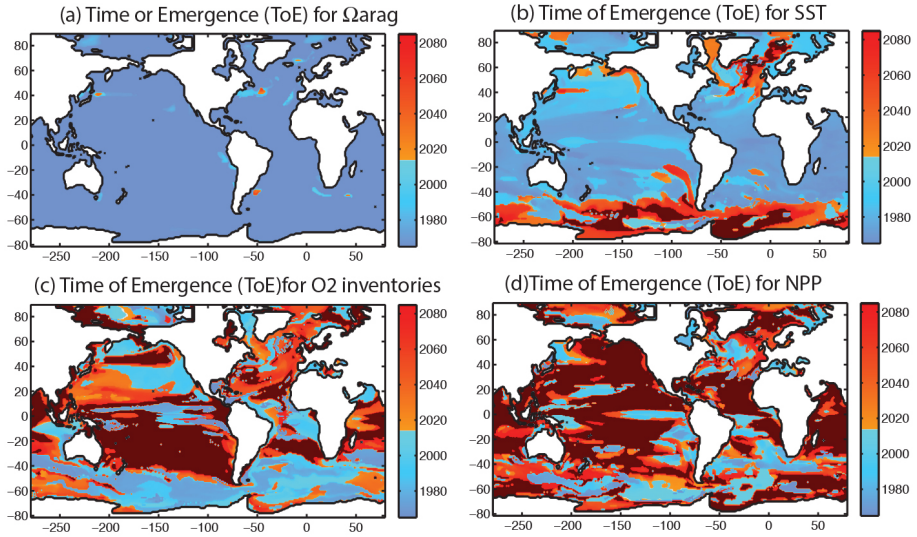

Figure 6. Time of Emergence (ToE), calculated using a threshold of one standard deviation (67 % confidence) for **(a)** Ω_{arag}, **(b)** SST, **(c)** O_2 inventories, and **(d)** NPP. The color scheme has been chosen to distinguish between relative to the present (2014) with warm colors indicating a ToE post-2014 and cold colors indicating a ToE pre-2014.

BGD
11, 18189–18227, 2014

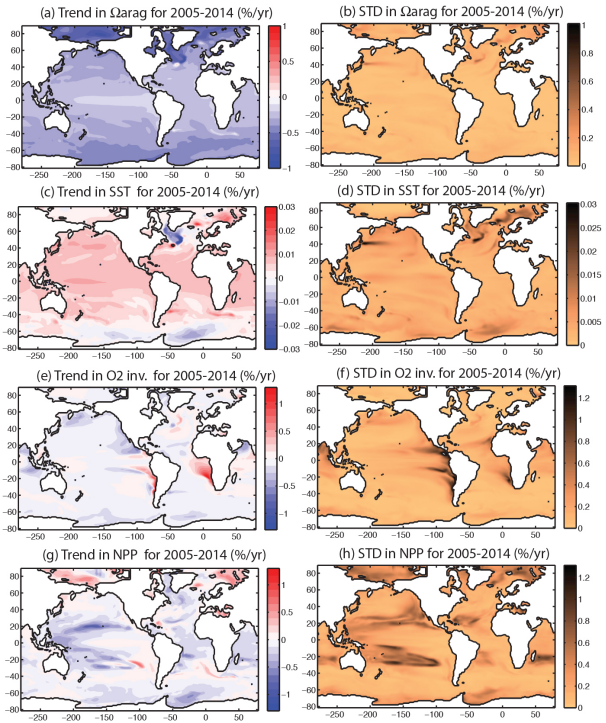

Figure A.1. Linear trends (left) and standard deviations of the linear trends (right) for **(a–b)** Ω_{arag}, **(c–d)** SST, **(e–f)** O_2 inventories from 100–600 m, and **(g–h)** net primary production averaged over 2005–2014. All fields are calculated using 30 yr trend windows, and the trends are shown in units of $\%/yr^{-1}$.

BGD
11, 18189–18227, 2014

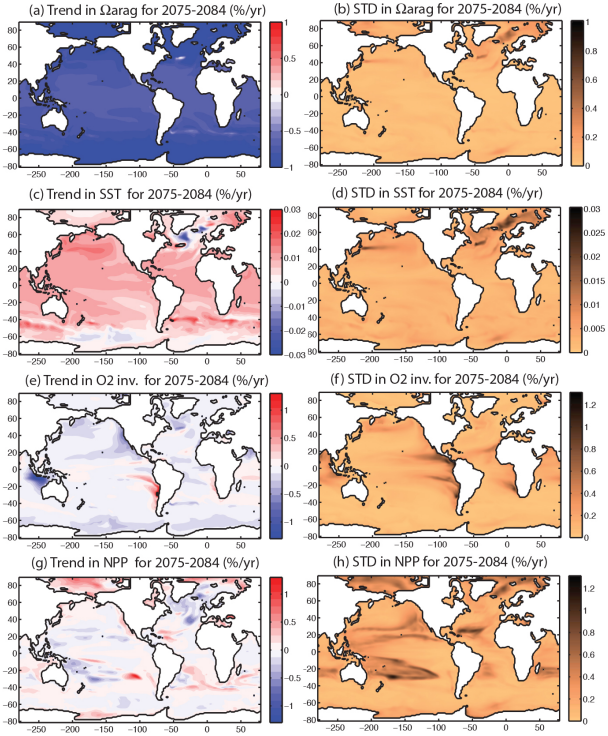

Figure A.2. Same as Fig. A1, but averaged over 2075–2084.

BGD
11, 18189–18227, 2014

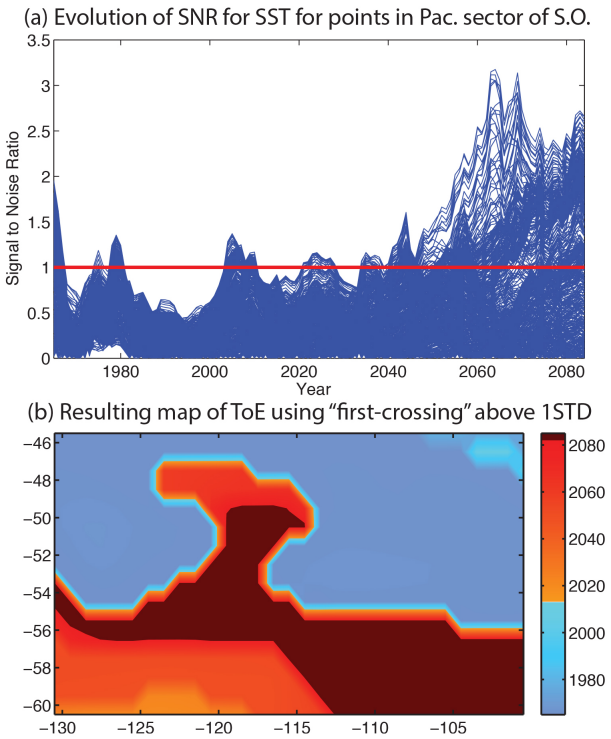

Figure A.3. Time of emergence of SST considered for a boxed region of the Pacific sector of the Southern Ocean (130–100° W and 45–60° S). The SNR calculated individually using annual mean SST for each gridpoint in the domain is shown in panel **(a)**, where a 30 yr window is used to calculated TREND and NOISE. Short timescale excursions of less than ten years are in evidence in modulations of maximum SNR. The spatial pattern of ToE for SST over this region is shown in panel **(b)**. A ToE before the present time (pre-2014) is indicated by cool (blue) colors, while a later ToE is indicated with warm (orange) colors. Saturation (ToE post-2085) is represented with maroon color.

BGD
11, 18189–18227, 2014

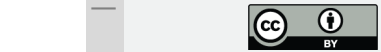

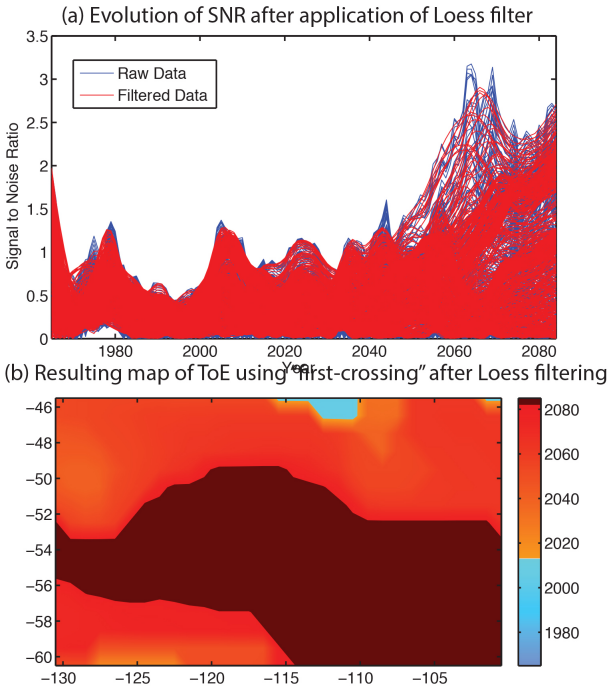

Figure A.4. The ToE is considered for the same region, but this time with application of a robust Loess filter with a tolerance window of ten years applied to the SNR of SST calculated for the individual surface grid points in the domain. The SNR after application of the robust Loess filter is shown in panel **(a)** in red, superposed over the same blue time series considered in Fig. A3a. The filtering effect on the short timescale maximum excursions of the SNR is evident in the Fig. The net effect over the full domain of the robust Loess filter is shown in panel **(b)**, revealing a later ToE over significant portions of the region of interest.

BGD
11, 18189–18227, 2014

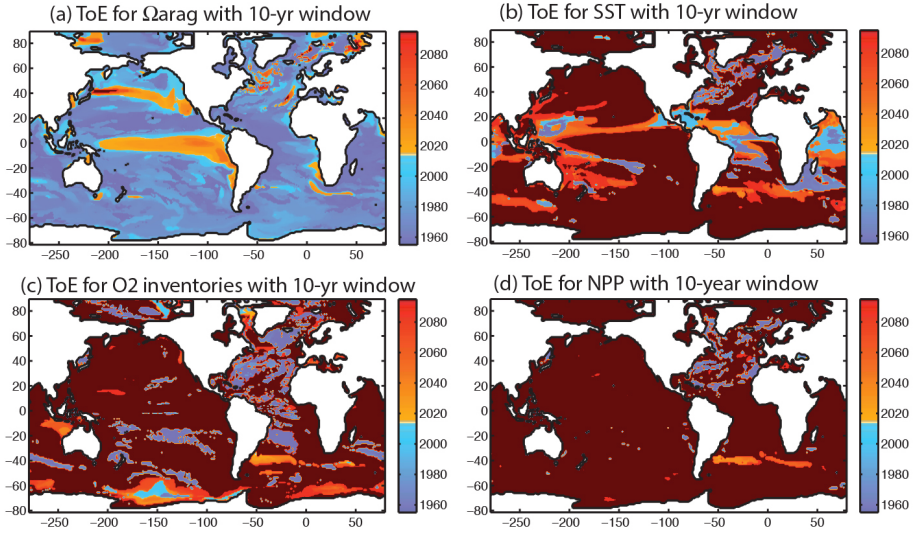

Figure A.5. The Time of Emergence (ToE) for each of the four ecosystem drivers has been calculated using a 10 yr window for the calculation of trends, considering the time interval 1955–2095. This is the complement to the results with ToE for a 30 yr window, shown in Fig. 6.

BGD
11, 18189–18227, 2014

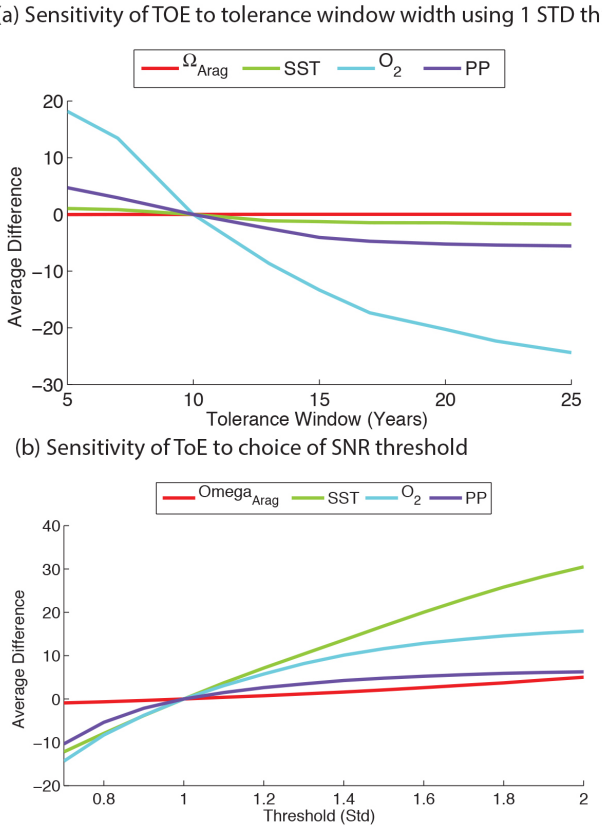

Figure A.6. Sensitivity analysis for tolerance window width in years (left) – using a one standard deviation threshold and considered around a 10 yr window, as well as a threshold level (right) – using a 10 year tolerance window and considered around a standard deviation of one. Caveats regarding averaging over fields that experience saturation are discussed in the text of the Supplementary Materials.

BGD
11, 18189–18227, 2014